One-Pot Preparation of FeSe-WSe_2 Composite and the Performance of Photo Fenton to Degradation Methylene Blue

[1]Chongchong Yan, [2]Wenxiang Zhao, [2]Jinyu Zhou, [1]Yanan Liu and [1]Jun Wan*

[1]College of Environment and Safety Engineering, Qingdao University of Science and Technology, Qingdao 266042, China.

[2]China Coal Technology& Engineering Group Nanjing Design& Research Institute Co. Ltd., Nanjing 210031, China.

wanjundz@sohu.com*

Summary: FeSe-WSe_2 composite photocatalyst was synthesized by a facile one-pot hydrothermal reaction with WSe_2, sodium selenite (Na_2SeO_3), hydrazine hydrate ($N_2H_4 \cdot H_2O$), hydrochloric acid (HCl), and Ferric chloride ($FeCl_3$). Different ratios of FeSe-WSe_2 composite photocatalysts were synthesized according to different Fe content, and FeSe-WSe_2 was characterized by XRD, SEM, UV-vis DRS and XPS. At the same time, the photocatalytic performance and catalytic mechanism of the composite photocatalyst were explored through the degradation of methylene blue (MB) by the composite. The experimental results show that under the best experimental conditions, the 37at% (Atomic ratio) FeSe-WSe_2 composite has the best removal effect on MB solution, and the removal rate reaches 99.8%. This shows that there is a synergistic effect of photocatalysis and Fenton reaction, which greatly improves the degradation ability of pollutants of FeSe-WSe_2. Since the degradation of pollutants by photo Fenton is carried out under neutral conditions, it is more conducive to future applications in actual production.

Keywords: Tungsten selenide; Iron selenide; Photo-Fenton; Photocatalyst; Methylene blue.

Introduction

The particularity of the advanced oxidation process (AOP) is mainly based on the hydroxyl radical (·OH) generated by redox, which has a high potential (2.80 V) and can degrade various refractory organic pollutants [1-4]. Because of its rapid formation and high degradation efficiency, the Fenton process has received widespread attention [1, 5-7]. However, the Fenton homogeneous process is not only affected by pH value but also limited by ferric hydroxide sludge [8-10].

To expand the application of Fenton reagents, the process of heterogeneous Fenton was developed. This is because organic compounds will be fully mineralized at ambient temperature[11]. Therefore, researchers have done a lot of research on the preparation and application of Fenton materials [12-19]. Among them, Photo-Fenton is an effective way to treat wastewater [20-24]. In the past few decades, the study of the heterogeneous Fenton process of the decomposition of organic pollutants under ultraviolet light has attracted widespread attention[25]. However, the practical application of the UV-based photo-Fenton method is limited because UV only accounts for 3%-5% of solar energy. Therefore, compared to artificial ultraviolet rays, the method of using solar light to catalyze the decomposition of organic pollutants may be very economical. Therefore, the development of optical Fenton catalyst plays an important role in actual production [26].

Visible light driving needs to be considered with the sensitivity of the catalyst to visible light and its light absorption ability. The efficient and stable photocatalyst is one of the necessary conditions for the further development and application of Fenton technology [27-29]. Some metal oxides had been researched and developed as visible light photocatalysts. The photocatalytic activity of the photocatalyst is attributed to the ability of the photocatalyst to generate electron-hole pairs determines [30, 31]. To improve the performance of

*To whom all correspondence should be addressed.

the catalyst, the researchers increased the number of active sites and doped additional transition metal atoms into the metal catalyst to stimulate electrocatalytic activity. For example, doping other atoms on graphene gives the composite material of huge surface area, high conductivity, and unique structure.

Transition metal-carbon disulfide (TMD) is currently one of the more desirable co-catalysts because of its greater chemical stability, faster charge migration, and efficient light absorption characteristics. In this regard, tungsten diselenide has attracted a lot of attention from researchers due to its special point and transport properties and superior electrical conductivity [32]. In the meantime, fluorescent nano-semiconductors made from iron-sulphur-based compounds nanomaterials have unique optical and electrical properties that also promote their application in bio-imaging and solar energy conversion [33]. Iron diselenide has narrow band gap energy and good conductivity, so it occupies a great advantage in industrial production [34].

In this paper, a new type of photocatalyst FeSe-WSe_2 was synthesized by a one-pot thermal method. Under visible light, the photo-Fenton reaction was carried out to degrade MB to explore the performance of the photocatalyst.

Experimental

Chemicals

Tungsten selenide (WSe_2) was brought from Macklin; Methylene blue (MB) and Ferric chloride ($FeCl_3$) were brought from China Shanghai Aladdin Chemical Reagent Co., Ltd. Sodium selenite (Na_2SeO_3) and ethanolamine were bought from Sinopharm Chemical Reagent Co., Ltd. Hydrazine Hydrate($N_2H_4 \cdot H_2O$) was purchased from Tianjin Sanhe Fine Chemical Co., Ltd.

Preparation of FeSe-WSe_2

Take 0.16 g $FeCl_3$ and 0.11 g WSe_2 to 6mLwater, and stirred for 30 min, then added 0.45g sodium selenite (Na_2SeO_3), 24 mL ethanolamine, and 8.5 mL hydrazine hydrate to the dispersed solution. The solution was reacted for 24 hours in a high-temperature oven at 140 °C. The sample is sealed and stored after washing and filtering.

Photocatalysis and photo-Fenton catalysis experiments

The light source in the photodegradation process is a xenon lamp with a wavelength greater than 420 nm. Disperse 0.05 g sample into 50 mL MB (20 mg/L) solution. Stir for 0.5 h under dark conditions to reach adsorption equilibrium. After the adsorption equilibrium, turn on the light source for photoreaction. Take a sample every 10 minutes to measure the absorbance. Then, calculate the MB concentration and removal rate according to the standard curve formula. Experiments are conducted by changing the ratio of the complex, the Fe to H_2O_2, and the pH.

Repeat cycle experiment

Under the 420 nm light irradiation, the stability and reusability of the photocatalyst were studied through five repeated cycles of photo-Fenton reaction in MB.

Characterization

The microstructure and element distribution of catalyst were characterized the by scanning electron microscope (SEM, JSM-6700F). X-ray photoelectron spectroscopy (XPS Thermo ESCALAB Xi) was used to characterize the atomic state of the complex. X-ray diffraction analyzer (XRD, D/MAX-2500/PC, Japanese Physics) is used for sample crystal characterization.

Results and Discussion

Material characterization

It can be seen from the scanning electron micrograph of FeSe in Fig. 1(a) that FeSe is in the form of small particles of uniform size, agglomerated together, and the small particles are uniform and the same in size. And Fig. 1(a) does not contain other morphological substances, which shows that the FeSe sample prepared in the experiment has good purity and good quality. In Fig. 1(b), it can be seen that many small particles growing on the columnar WSe_2 column. The appearance and shape of this small particle are consistent with Fig. 1(a). At the same time, the element distribution characterization of the composite material was carried out to further indicate the distribution state of each element in the synthesized sample. Fig. 1(c)(d) and (e) is the distribution diagram of the elements corresponding to Fe, W, and Se in the composite. From the figure, it can be seen that the distribution of each element is dense and uniform. The EDS spectrum (f) of FeSe-WSe_2 also shows the presence of various elements.

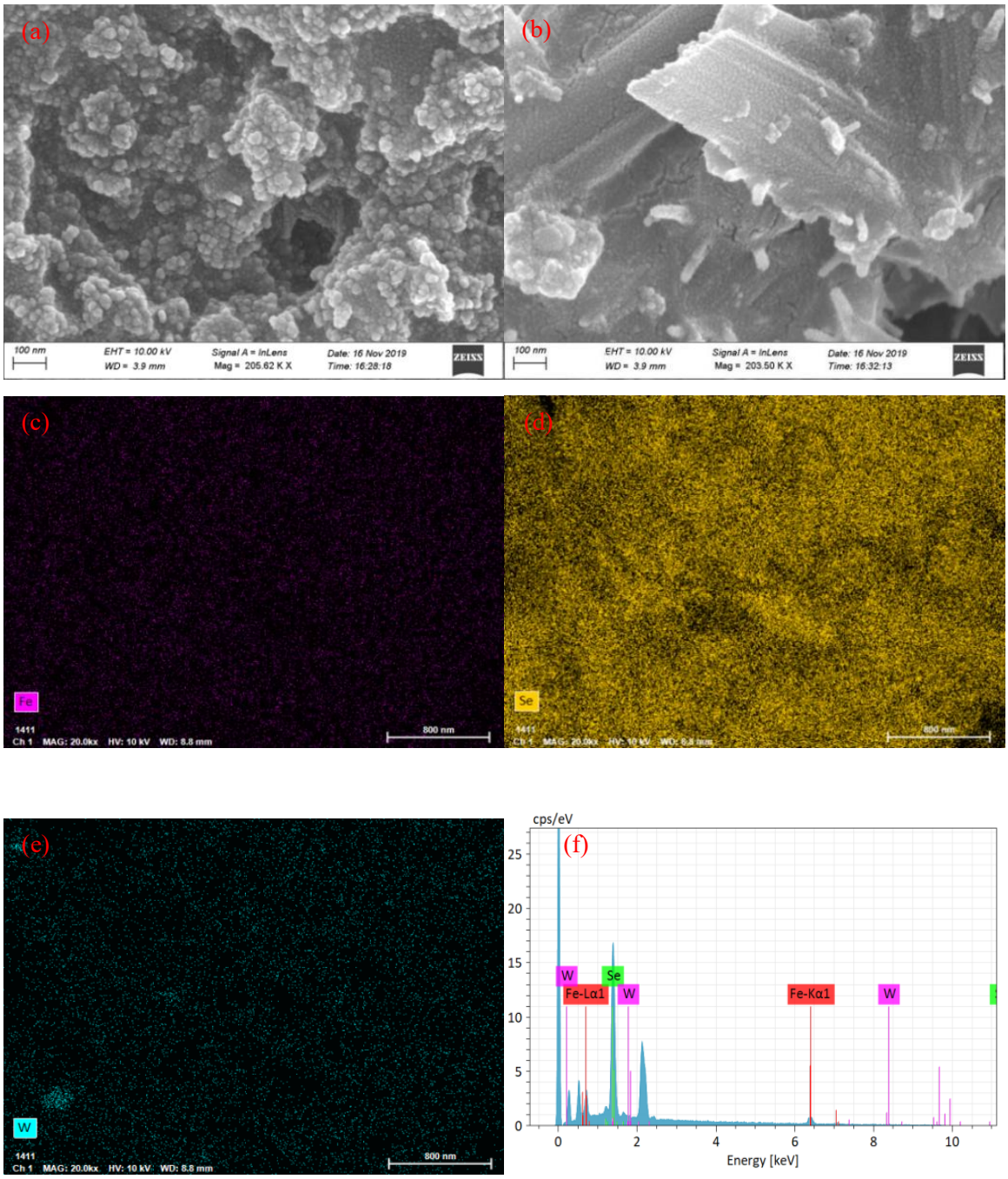

Fig. 1: SEM of FeSe(a),FeSe-WSe_2(b), elemental mapping images of Fe(c),W(d),Se(e) and EDS of FeSe-WSe_2

Table-1: The content of each atom in FeSe-WSe_2.

Element	Relative atomic mass	Quality(%)	Atomic ratio(%)
Fe	55.8	11.7	36.6
W	183.8	38.6	8.9
Se	78.9	49.7	54.5
	total	100	100

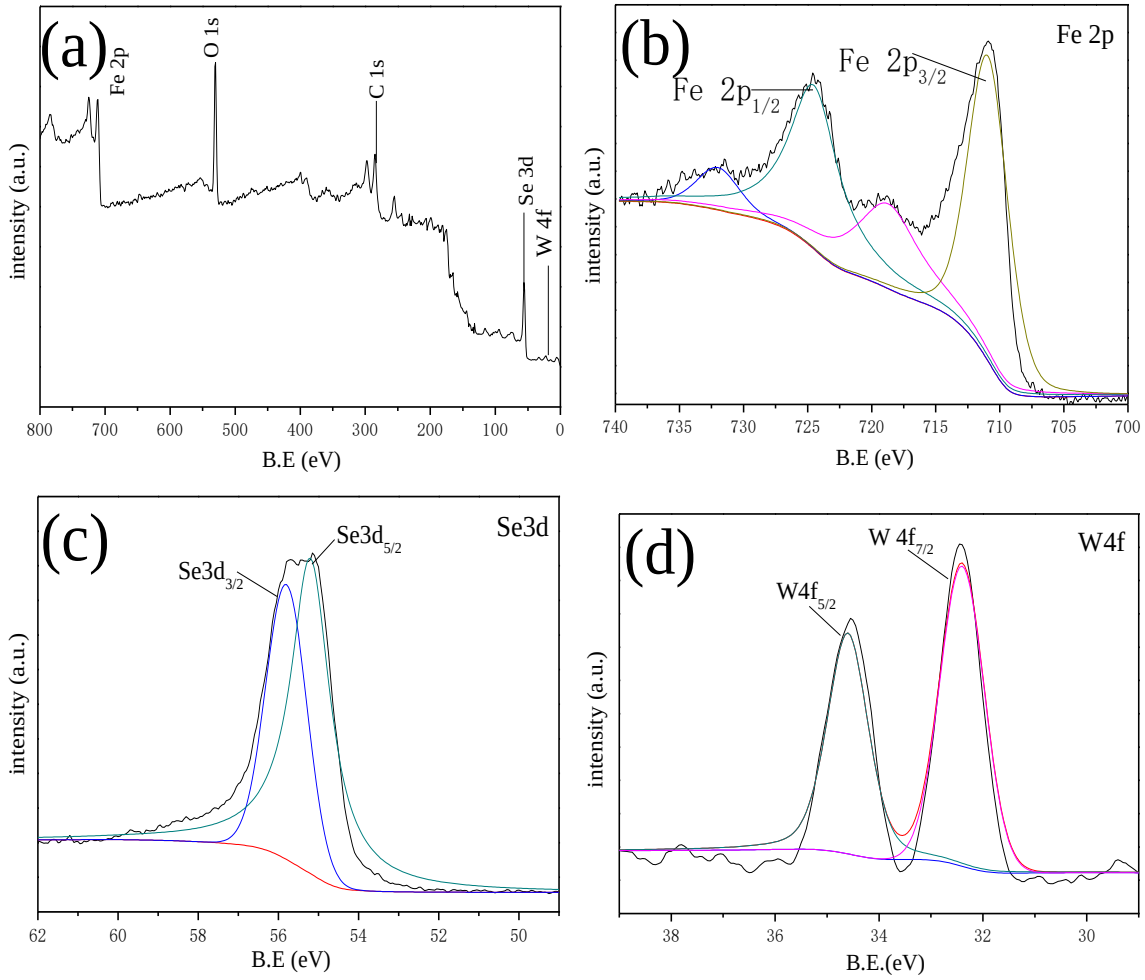

Fig. 2: XPS diagram of the complex (a). Atomic energy spectrum of Fe 2p(b), Se 3d (c), and W 4f (d) in the FeSe-WSe_2 composite.

Table 1 is the comparison of the content of each element of the composite. The above electron microscopy and element characterization all show that the synthesized composite sample is uniform and free of other impurities.

XPS was used to characterize the composite to determine the atomic composition and morphology of the FeSe-WSe_2 surface. Fig. 2(a) can see the existence of the five elements and their corresponding peak positions. Among them, carbon and oxygen atoms are the backgrounds of the process of testing samples, so the carbon and oxygen atom summits appear in the full spectrum. Fig. 2(b) is the electron energy spectrum of the iron atom. The peak positions at 711.1 eV and 724.5 eV are attributed to the peaks of Fe $2p_{3/2}$ and Fe $2p_{1/2}$. 711.1 eV is belong to the original structure of the iron species, which belongs to the selenium iron ore lattice and the iron species with a higher oxidation state. The peak at 718.8 eV is derived from the binding energy of Fe(II) and Se atoms. The peak at 731.8 eV is attributed to the satellite peak of Fe $2p_{1/2}$[34, 35]. Fig. 2(c) is the electron energy spectrum of the Se atom. The peak at 55.2 eV and 55.9 eV may be Se $3d_{5/2}$ and Se $3d_{3/2}$, which indicate the existence of FeSe and WSe_2. It is seen in Fig. 2(d) that the peak positions of 32.4 eV and 34.6 eV correspond to W $4f_{7/2}$ and W $4f_{5/2}$. Through the electron energy spectrum analysis of all the above atoms, it can clearly show the existing state of the atoms in the complex, and it is consistent with the literature report.

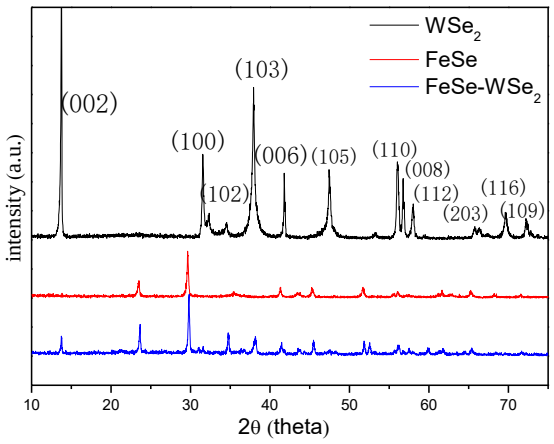

Fig. 3: XRD pattern of WSe_2, FeSe, FeSe-WSe_2.

Fig. 3 is the X-ray diffraction comparison diagram of WSe_2, FeSe, and FeSe-WSe_2. Major characteristic peaks of WSe_2 and the corresponding crystal planes can be seen in the figure. The angles and corresponding crystal planes in the figure are the standard PDF card (JCPDS#38-1388) of WSe_2 that is consistent. It can be seen from the figure that the angles of FeSe at 24.1°, 29.8°, 41.2°, 45.5°, 52.5°, 55.1°, 62.3°, 68.8° correspond to (100) (101) (102) (110) (200) (201) (202) (104) plane. This is consistent with the main peak position shown on the standard card (JCPDS#65-9125). This indicates that the prepared sample is FeSe. In addition, there are fewer spurious peaks and sharp peaks, indicating that the purity of the prepared sample is good. This indicates that the prepared sample is FeSe. In addition, there are fewer spurious peaks and sharp peaks, indicating that the purity of the prepared sample is good. And from the XRD diagram of the FeSe-WSe_2 composite, the characteristic peaks of WSe_2 and FeSe are all present in the composite FeSe-WSe_2, and the angle corresponding to the characteristic band can be seen in the figure. Although the WSe_2 peak in the composite is relatively weak due to the low content of WSe_2, the corresponding WSe_2 peak position in the composite can still be seen. This shows that the synthesized sample is indeed FeSe-WSe_2.

The absorbance of the sample shows the absorption range of FeSe, WSe_2, and FeSe-WSe_2 by UV-vis spectrophotometer. As shown in Fig. 4(a): the absorption peak of FeSe and WSe_2 decreases sharply at 600-680 nm, and the light absorption capacity is weakened. FeSe-WSe_2 compensates for the light absorption range from 700 nm to 800 nm and increases the light absorption range. For crystalline semiconductors, the band gap can be estimated according to the Kubelka Munk equation. In Fig. 4(b), the estimated band gaps of FeSe, WSe_2 and FeSe-WSe_2 are approximately 2.6 eV, 1.3 eV and 1.2 eV. This is relatively similar to the band gap of FeSe reported in the relevant literature to be around 3.0 eV, and to the band gaps of 1.6 eV (monolayer) and 1.2 eV (multilayer) for WSe_2 in different morphologies, etc[36-39]. The band gap energy of composite materials is smaller than that of a single substance. When exposed to light, electrons are excited to produce electronic transitions. The results show that the composite catalytic material has a broader absorption base in the visible region and has better visible light absorption capacity. And it greatly improves the absorption and utilisation of solar energy, leading to an increase in the degradation efficiency of organic matter.

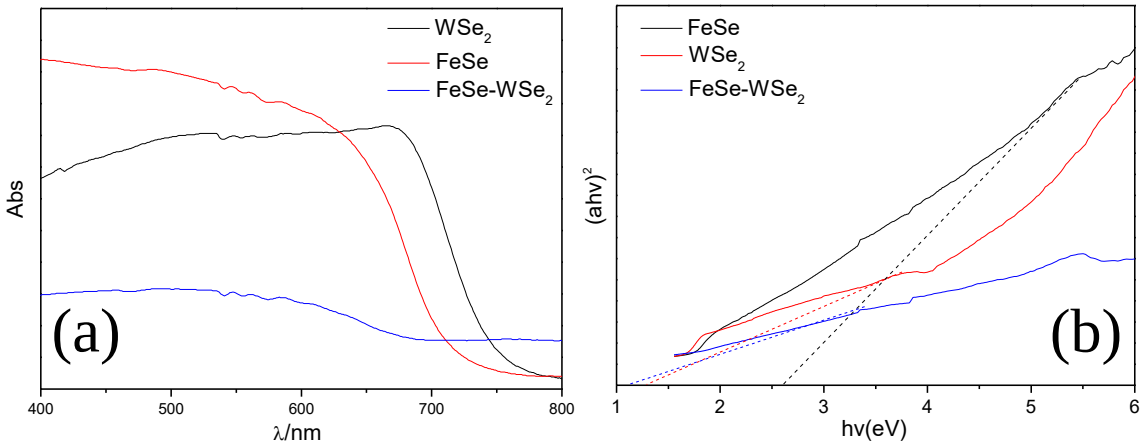

Fig. 4: UV-Vis absorption spectra (a) and estimated band gaps of FeSe, WSe_2 and FeSe-WSe_2 (b).

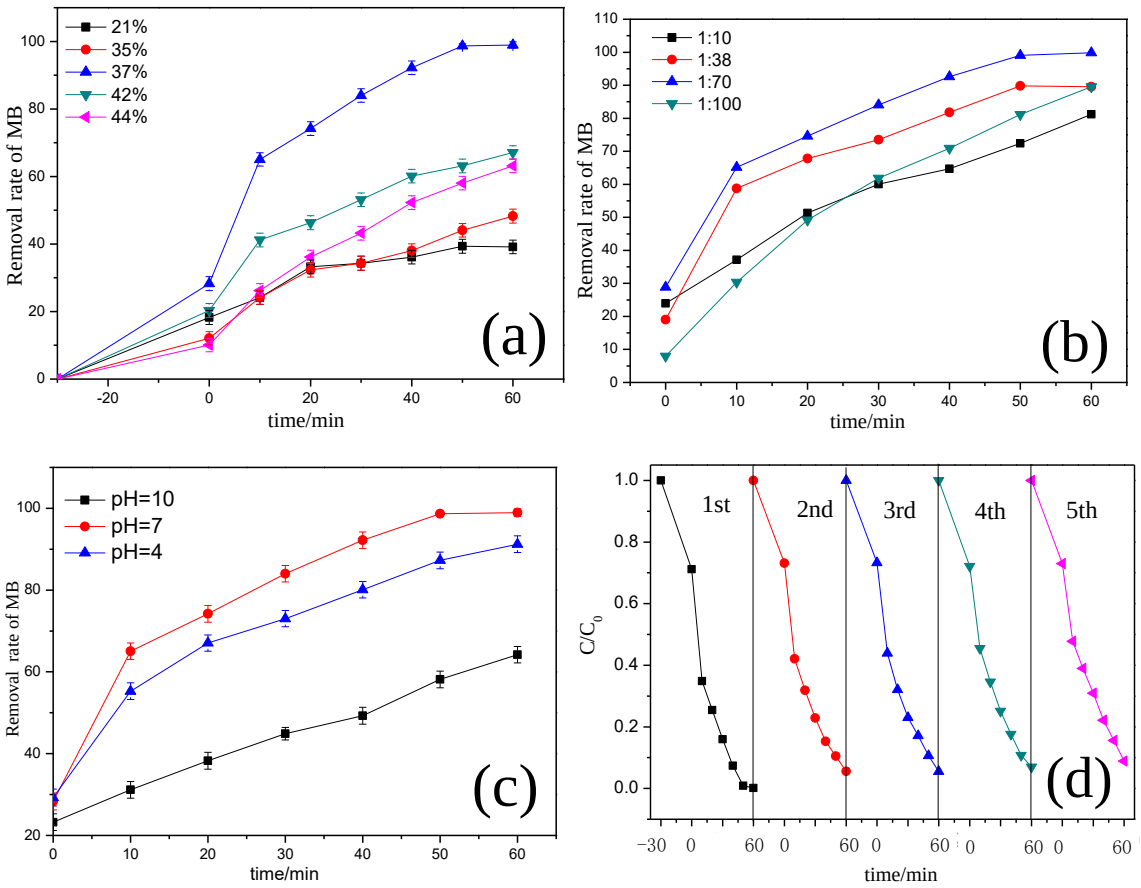

Fig. 5: Degradation curves of methyl bromide by catalysts with different iron mass ratios (a). Effect of different Fe to H_2O_2 mass ratios on photo-Fenton (b). Effect of different pH on MB degradation (c). Repeated recycling experiments of FeSe-WSe_2(d).

Properties of FeSe-WSe_2 nanocomposites

Under the same conditions, the ratio of Fe content (at%) and the ratio of Fe to H_2O_2 in the composite were investigated by photocatalytic experiments. The removal rate of 37at% FeSe-WSe_2 is much higher and reaches 99.8% (see in Fig. 5a), which would attribute to the increases in Fe, the higher efficiency of the photo-Fenton reaction. When the proportion of Fe in FeSe-WSe_2 was more than 37%, the MB removal rate decreased. The reason is that a high concentration of Fe cannot fully participate in the optical photo-Fenton. At the same time, the influence of H_2O_2 on the effect of MB degradation in the Fenton reaction was also carried out. With the increases in H_2O_2 content, the effect of the photo-Fenton reaction to degrade MB gradually increased (see in Fig. 5b). When the ratio of H_2O_2 and Fe is 1:70, the optical Fenton effect is the best.

Generally, the Fenton reaction has a better redox degradation effect within a suitable pH range. Under the conditions of pH = 4, 7, and 10, respectively, the same concentration of MB was degraded for exploration. As shown in Fig. 5(c), the removal rates of MB at pH = 4 and 10 are 91.7% and 64.6%, respectively. When pH = 7, the composite has the best removal effect on MB. Compared with acidic or alkaline conditions, neutral conditions have a better removal effect and are more convenient for practical applications. Through five repeated cycles of the composite degrading MB experiment, to show the stability and repeatability of the FeSe-WSe_2 composite photocatalyst. As shown in Fig. 5(d), with the increase in the number of photocatalytic experiments, the photocatalytic degradation efficiency of the composites stabilized above 85%. This shows that the FeSe-WSe_2 composite material has excellent stability. Repeated use of photocatalysts reduces the waste of samples and preparation materials and saves resources for sustainable development.

TiO_2, FeSe, WSe_2, and FeSe-WSe_2 were used to degradate the MB for comparison photocatalytic performance under the same conditions. The degradation effect was shown in Fig. 6(a). The adsorption of FeSe or WSe_2 is weak, and the adsorption capacity of the composite material FeSe-WSe_2 is improved. The overall photocatalytic effect of TiO_2 and WSe_2 is weak, and the degradation efficiency of MB is only 42.2% and 17.7%. The removal efficiency of FeSe and FeSe-WSe_2 is 82.0% and 99.8%. The adsorption ability and photocatalytic reaction of the composite material were all improved. Fig. 6(b) shows the photodegradation kinetics of different substances on MB. The photodegradation rate of FeSe-WSe_2 composite material is 0.06918 min^{-1}, which is significantly higher than the reaction rate of WSe_2, FeSe, and TiO_2.

By comparing with the published optical Fenton article, the superiority of the material performance of this article is further explained. As shown in Table 2, the degradation experimental conditions and removal rate of different substances on MB were also compared. The FeSe-WSe_2 has certain advantages in terms of the concentration, reaction time, and dosage of MB degradation.

The mechanism of FeSe-WSe_2 degradation of MB was also deduced. At present, in numerous literature reports, FeSe is called an effective promoter [44, 45], and Fe^{2+} in the composite undergoes high-valent oxidation reactions. The two reaction processes are carried out simultaneously with efficient and speed of degradation of pollutants. The conduction band and valence band are calculated according to the following equations: $E_{CB} = \chi - E_e - 0.5E_g$ and $E_{VB} = E_{CB} + E_g$, where E_{CB} is the CB edge potential, χ is the electronegativity of the semiconductor, E_e is the energy of the free electron on the hydrogen scale (~4.5 eV), E_g is the band gap and E_{VB} is the VB edge potential[46].

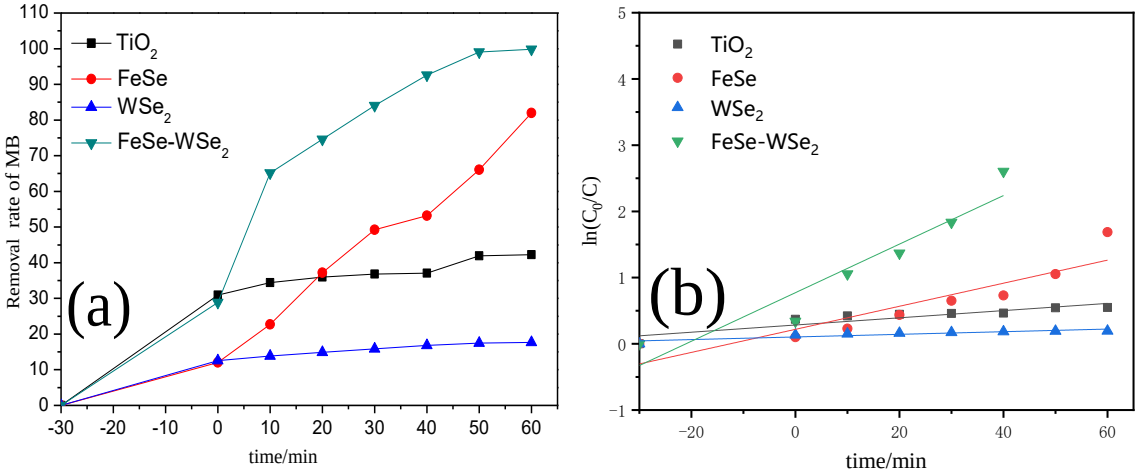

Fig. 6: Comparison of different substances on MB (Mass ratio of Fe 37%at, Fe to H_2O_2 ratio 1:70, catalyst dosage 0.05 g, MB initial concentration 6.0×10^{-5} mol/L, pH=7) (a) and kinetics of different catalysts on MB(b).

Table 2 Compare the removal effect of other photo-Fenton reactions on MB.

Material	Light region	MBconcentration(mg/L)	Volume (mL)	Dosingamount (g)	reaction time (min)	Removal rate (%)	Reference
Mn_3O_4@ZnO/ACFs	visible	5	80	0.025	150	close to 100	[40]
$Fe_\alpha Bi1-_\alpha OBr/Fe_3O_4/Mn_3O_4$	visible	10	100	0.1	80	98	[41]
Fe_3O_4/CuO	——	10	50	0.05	120	94	[42]
FeOOH/Bi_2WO_6	visible	12	20	0.02	48	98	[43]
FeSe-WSe_2	visible	20	50	0.05	90	99.8	This work

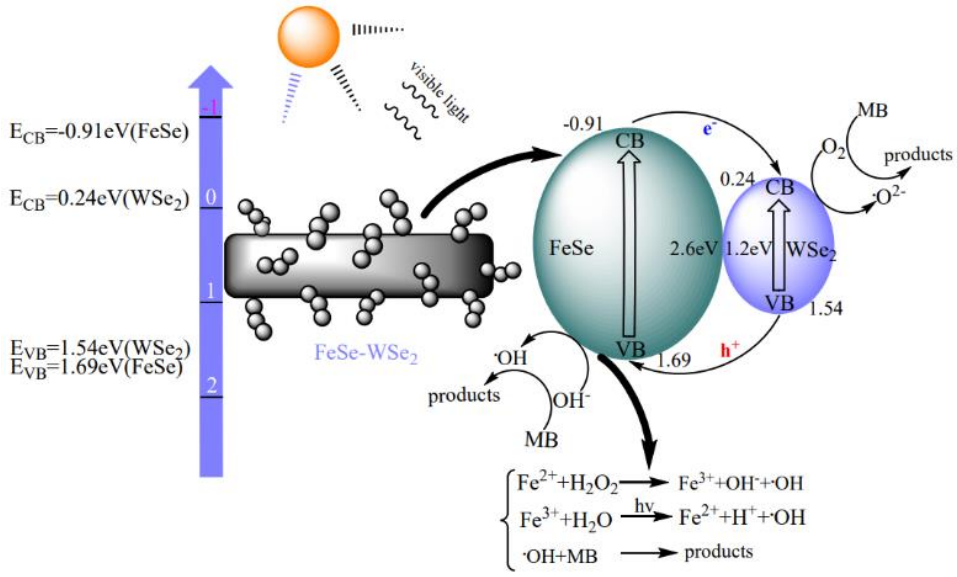

Fig. 7: Photocatalytic mechanism of FeSe-WSe_2.

As shown in Fig. 7, the conduction band (CB) and valence band (VB) of FeSe are -0.91 eV and 1.69 eV, and the conduction band (CB) and valence band (VB) of WSe_2 are 0.24 eV and 1.54 eV, which can be calculated from the equation in the previous paragraph. Under visible light, electrons in FeSe are excited from the valence band (VB) to transition to the conduction band (CB) and continue to migrate to the surface of the promoter WSe_2. The photogenerated electrons (e^-) on WSe_2 react with O_2 to generate O^{2-}, and the electron holes (h^+) are transferred from the VB of WSe_2 to the VB of FeSe. The h^+ on the surface of FeSe reacts with adsorbed water and hydroxide to generate ·OH. FeSe particles can reduce the electron-hole recombination rate in WSe_2, and act as a promoter to greatly improve the photocatalytic activity of WSe_2 [45]. At the same time, during the photocatalytic reaction, Fe^{2+} and H_2O_2 in FeSe-WSe_2 undergo advanced oxidation reactions: first, Fe^{2+} reacts with hydrogen peroxide to form Fe^{3+}, ·OH, and OH^-. Secondly, Fe^{3+} is reduced to Fe^{2+} H_2O, and ·OH under a light. Finally, ·OH and MB redox and degrade pollutants. The above two reactions proceed simultaneously and cooperate, which greatly improves the effect of FeSe-WSe_2 in degrading pollutants [47-49]. The removal rate of pollutants is much higher than that of a single substance, and the reaction rate of the entire photocatalytic process is improved.

Conclusions

The FeSe-WSe_2 was synthesized by the hydrothermal method. The carrier transport of FeSe-WSe_2 heterostructure can be carried out in the composite to obtain long service life and higher separation efficiency. At the same time, the Fe^{2+} in the composite undergoes advanced oxidation reactions, and the two reactions cooperate to accelerate the rate of degradation of pollutants. This makes the 37at%FeSe-WSe_2 composite photocatalyst have high efficiency and excellent photocatalytic performance.

Acknowledgements

This work was supported by Independent Scientific Research Project of Nanjing Design Institute Co., LTD., China Coal Technology & Engineering Group (ZL21-KY04).

Declaration of Interest Statement

The authors declare that they have no conflict of interest.

References

1. Y. Zhou, L. Zhou, Y. Zhou, M. Xing and J. Zhang, Z-scheme photo-Fenton system for efficiency synchronous oxidation of organic contaminants and reduction of metal ions, *Appl. Catal. B Environ.*, **279**: 119365(2020).
2. A. L. Zhu, Y. Y. Guo, G. L. Liu, M. Y. Song, Y. Liang, Y. Cai and Y. G. Yin, Hydroxyl radical formation upon dark oxidation of reduced iron minerals: Effects of iron species and

environmental factors, *Chinese Chem. Lett.*, **30**: 2241-2244(2019).

3. J. Jiang, X. Wang, Y. Liu, Y. Ma, T. Li, Y. Lin, T. Xie and S. Dong, Photo-Fenton degradation of emerging pollutants over Fe-POM nanoparticle/porous and ultrathin g-C_3N_4 nanosheet with rich nitrogen defect: Degradation mechanism, pathways, and products toxicity assessment, *Appl. Catal. B Environ.*, **278**: 119349(2020).
4. A. Ghaffar, L. Zhang, X. Zhu and B. Chen, Porous PVdF/GO Nanofibrous Membranes for Selective Separation and Recycling of Charged Organic Dyes from Water, *Environ. Sci. Technol.*, **52**: 4265-4274(2018).
5. Z. Yang, X. Zhang, S. Pu, R. Ni, Y. Lin and Y. Liu, Novel Fenton-like system (Mg/Fe-O_2) for the degradation of 4-chlorophenol, *Environ. Pollut.*, **250**: 906-913(2019).
6. Q. Yi, J. Ji, B. Shen, C. Dong and M. Xing, Singlet Oxygen Triggered by Superoxide Radicals in a Molybdenum Cocatalytic Fenton Reaction with Enhanced REDOX Activity in the Environment, *Environ. Sci. Technol.*, **53**: 9725-9733(2019).
7. C. Dong, J. Ji, B. Shen, M. Xing and J. Zhang, Enhancement of H_2O_2 Decomposition by the Cocatalytic Effect of WS_2 on the Fenton Reaction for the Synchronous Reduction of Cr(VI) and Remediation of Phenol, *Environ. Sci. Technol.*, **52**: 11297-11308(2018).
8. Y. Zhu, R. Zhu, Y. Xi, T. Xu, L. Yan, J. Zhu, G. Zhu and H. He, Heterogeneous photo-Fenton degradation of bisphenol A over Ag/AgCl/ferrihydrite catalysts under visible light, *Chem. Eng. J.*, **346**: 567-577(2018).
9. G. Subramanian and G. Madras, Remarkable enhancement of Fenton degradation at a wide pH range promoted by thioglycolic acid, *Chem. Commun.*, **53**: 1136-1139(2016).
10. X. Li, S. Liu, D. Cao, R. Mao and X. Zhao, Synergetic activation of H_2O_2 by photo-generated electrons and cathodic Fenton reaction for enhanced self-driven photoelectrocatalytic degradation of organic pollutants, *Appl. Catal. B Environ.*, **235**: 1-8(2018).
11. Q. Feng, S. Li, W. Ma, H.-J. Fan, X. Wan, Y. Lei, Z. Chen, J. Yang and B. Qin, Synthesis and characterization of Fe_3O_4/ZnO-GO nanocomposites with improved photocatalytic degradation methyl orange under visible light irradiation, *J. Alloy. Compd.*, **737**: 197-206(2018).
12. S. Sun, H. Yao, W. Fu, S. Xue and W. Zhang, Enhanced degradation of antibiotics by photo-fenton reactive membrane filtration, *J Hazard Mater*, **386**: 121955(2020).
13. A. Della-Flora, M. L. Wilde, P. S. Thue, D. Lima, E. C. Lima and C. Sirtori, Combination of solar photo-Fenton and adsorption process for removal of the anticancer drug Flutamide and its transformation products from hospital wastewater, *J Hazard Mater*, **396**: 122699(2020).
14. A. Pulgarin, S. Giannakis, C. Pulgarin, C. Ludwig and D. Refardt, A novel proposition for a citrate-modified photo-Fenton process against bacterial contamination of microalgae cultures, *Appl. Catal. B Environ.*, **265**: 118615(2020).
15. E. Rommozzi, S. Giannakis, R. Giovannetti, D. Vione and C. Pulgarin, Detrimental vs. beneficial influence of ions during solar (SODIS) and photo-Fenton disinfection of E. coli in water: (Bi)carbonate, chloride, nitrate and nitrite effects, *Appl. Catal. B Environ.*, **270**: 118877(2020).
16. S. Agrawal, N. Nirwan and A. Chohadia, Degradation of acriflavine using environmentally benign process involving singlet-oxygen-photo-Fenton: A comparative study, *J. Photoch. Photobio. A*, **398**: 112547(2020).
17. A. Wang, Z. Chen, Z. Zheng, H. Xu, H. Wang, K. Hu and K. Yan, Remarkably enhanced sulfate radical-based photo-Fenton-like degradation of levofloxacin using the reduced mesoporous MnO@MnOx microspheres, *Chem. Eng. J.*, **379**: 122340(2020).
18. X. Huang, N. Zhu, F. Mao, Y. Ding, S. Zhang, H. Liu, F. Li, P. Wu, Z. Dang and Y. Ke, Enhanced heterogeneous photo-Fenton catalytic degradation of tetracycline over yCeO_2/Fh composites: Performance, degradation pathways, Fe^{2+} regeneration and mechanism, *Chem. Eng. J.*, **392**: 123636(2020).
19. C. Casado, J. Moreno-SanSegundo, I. De la Obra, B. Esteban García, J. Antonio Sánchez Pérez and J. Marugán, Mechanistic modelling of wastewater disinfection by the photo-Fenton process at circumneutral pH, *Chem. Eng. J.*, **403**: 126335(2020).
20. Y. Li, G. Wei, L. Shao, Z. Li, F. Yu, J. Liu, X. Yang, Q. Lu, A. Li and Y. Huang, Green synthesis of red mud based ZnOFe_2O_3 composite used for photo-Fenton reaction under visible light, *J. Clean. Prod.*, **207**: 717-727(2019).
21. N. P. F. Gonçalves, M. Minella, D. Fabbri, P. Calza, C. Malitesta, E. Mazzotta and A. Bianco Prevot, Humic acid coated magnetic particles as highly efficient heterogeneous photo-Fenton materials for wastewater treatments, *Chem. Eng. J.*, **390**: 124619(2020).

22. Y. Zhao, S. Kang, L. Qin, W. Wang, T. Zhang, S. Song and S. Komarneni, Self-assembled gels of Fe-chitosan/montmorillonite nanosheets: Dye degradation by the synergistic effect of adsorption and photo-Fenton reaction, *Chem. Eng. J.*, **379**: 122322(2020).
23. Y. Zhou, Y. Gao, S. Y. Pang, J. Jiang, Y. Yang, J. Ma, Y. Yang, J. Duan and Q. Guo, Oxidation of fluoroquinolone antibiotics by peroxymonosulfate without activation: Kinetics, products, and antibacterial deactivation, *Water Res.*, **145**: 210-219(2018).
24. X. Wang, A. Wang and J. Ma, Visible-light-driven photocatalytic removal of antibiotics by newly designed C_3N_4@$MnFe_2O_4$-graphene nanocomposites, *J. Hazard. Mater.*, **336**: 81(2017).
25. Y. Liu, Y. Mao, X. Tang, Y. Xu, C. Li and F. Li, Synthesis of Ag/AgCl/Fe-S plasmonic catalyst for bisphenol A degradation in heterogeneous photo-Fenton system under visible light irradiation, *Chinese J. Catal.*, **38**: 1726-1735(2017).
26. G. Wei, Y. Yang, Y. Li, L. Zhang, Z. Xin, Z. Li and L. Huang, A new catalytic composite of bentonite-based bismuth ferrites with good response to visible light for photo-Fenton reaction: Preparation, characterization and analysis of physicochemical changes, *Appl. Clay Sci.*, **184**: 105397(2020).
27. A. V. Vorontsov, Advancing Fenton and photo-Fenton water treatment through the catalyst design, *J Hazard Mater*, **372**: 103-112(2019).
28. Z. Wang, C. Lai, L. Qin, Y. Fu, J. He, D. Huang, B. Li, M. Zhang, S. Liu, L. Li, W. Zhang, H. Yi, X. Liu and X. Zhou, ZIF-8-modified $MnFe_2O_4$ with high crystallinity and superior photo-Fenton catalytic activity by Zn-O-Fe structure for TC degradation, *Chem. Eng. J.*, **392**: 124851(2020).
29. M. Cheng, G. Zeng, D. Huang, C. Lai, P. Xu, C. Zhang and Y. Liu, Hydroxyl radicals based advanced oxidation processes (AOPs) for remediation of soils contaminated with organic compounds: a review, *Chem. Eng. J.*, **284**: 582-598(2016).
30. Q. J. Wang, Y. Cui, R. J. Huang, L. F. Zhong, P. Yan, S. L. Zhang, Q. H. Zhao, D. H. Jiang, A. D. Tang and H. M. Yang, A heterogeneous Fenton reaction system of N-doped TiO_2 anchored on sepiolite activates peroxymonosulfate under visible light irradiation, *Chem. Eng. J.*, **383**: 123142(2020).
31. M. Ahmad, X. Quan, S. Chen and H. T. Yu, Tuning Lewis acidity of MIL-88B-Fe with mix-valence coordinatively unsaturated iron centers on ultrathin Ti_3C_2 nanosheets for efficient photo Fenton reaction, *Appl. Catal. B Environ.*, **264**: 12(2020).
32. Y. P. Gao, X. Wu, K. J. Huang, L. L. Xing, Y. Y. Zhang and L. Liu, Two-dimensional transition metal diseleniums for energy storage application: a review of recent developments, *Crystengcomm*, **19**: 404-418(2017).
33. X. Mao, J. G. Kim, J. S. Han, H. S. Jung, S. G. Lee, N. A. Kotov and J. Lee, Phase-Pure FeSex (x=1, 2) Nanoparticles with One- and Two-Photon Luminescence, *J. Am. Chem. Soc.*, **136**: 7189-7192(2014).
34. X. Xu, Y. Ge, M. Wang, Z. Zhang, P. Dong, R. Baines, M. Ye and J. Shen, Cobalt-Doped $FeSe_2$-RGO as Highly Active and Stable Electrocatalysts for Hydrogen Evolution Reactions, *ACS Appl Mater. Inter.*, **8**: 18036-18042(2016).
35. C. Lv, H. Liu, D. Li, S. Chen, H. Zhang, X. She, X. Guo and D. Yang, Ultrafine FeSe nanoparticles embedded into 3D carbon nanofiber aerogels with FeSe/Carbon interface for efficient and long-life sodium storage, *Carbon*, **143**: 106-115(2019).
36. [36] S. B. Desai, G. Seol, J. S. Kang, H. Fang, C. Battaglia, R. Kapadia, J. W. Ager, J. Guo and A. Javey, Strain-Induced Indirect to Direct Bandgap Transition in Multi layer WSe_2, *Nano Lett.*, **14**: 4592-4597(2014).
37. K. Kim, S. Larentis, B. Fallahazad, K. Lee, J. M. Xue, D. C. Dillen, C. M. Corbet and E. Tutuc, Band Alignment in WSe2-Graphene Heterostructures, *Acs Nano*, **9**: 4527-4532(2015).
38. Luo H and F. J. K., The Il-VI semiconductor blue-green laser: challenges and solution, *Semicond. Sci. Tech.*, **10**: 1041(1995).
39. T. Roy, M. Tosun, M. Hettick, G. H. Ahn, C. M. Hu and A. Javey, 2D-2D tunneling field-effect transistors using WSe_2/$SnSe_2$ heterostructures, *Appl. Phys. Lett.*, **108**: 5(2016).
40. X. Cui, J. Li, D. H. L. Ng, J. Liu, Y. Liu and W. Yang, 3D hierarchical ACFs-based micromotors as efficient photo-Fenton-like catalysts, *Carbon*, **158**: 738-748(2020).
41. Y. Liu, J. Li, J. Li, X. Yan, F. Wang, W. Yang, D. H. L. Ng and J. Yang, Active magnetic Fe^{3+}-doped BiOBr micromotors as efficient solar photo-fenton catalyst, *J. Clean. Prod.*, **252**: 2020).
42. H. Ghasemi, B. Aghabarari, M. Alizadeh, A. Khanlarkhani and N. Abu-Zahra, High efficiency decolorization of wastewater by Fenton catalyst: Magnetic iron-copper hybrid oxides, *J. Water Process Eng.*, **37**: 101540(2020).
43. L. Guo, K. Zhang, X. Han, Q. Zhao, D. Wang, F. Fu and Y. Liang, Highly efficient visible-light-

driven photo-Fenton catalytic performance over FeOOH/Bi2WO6 composite for organic pollutant degradation, *J. Alloy. Compd.*, **816**: 152560(2020).

44. W. Zhong, W. Tu, S. Feng and A. Xu, Photocatalytic H_2 evolution on CdS nanoparticles by loading FeSe nanorods as co-catalyst under visible light irradiation, *J. Alloy. Compd.*, **772**: 669-674(2019).
45. X. Li, H. F. Jiao, X. Z. Shi, A. Sun, X. Wang, J. Chai, D. X. Li and J. Chen, Development and application of a novel fluorescent nanosensor based on FeSe quantum dots embedded silica molecularly imprinted polymer for the rapid optosensing of cyfluthrin, *Biosens Bioelectron*, **99**: 268-273(2018).
46. X. Chen, J. Zhang, J. H. Zeng, Y. X. Shi, G. Z. Huang, L. L. Zhang, H. B. Wang, Z. Kong, J. H. Xi and Z. G. Ji, Novel 3D/2D heterojunction photocatalysts constructed by three-dimensional In_2S_3 dandelions and ultrathin hexagonal SnS_2 nanosheets with excellent photocatalytic and photoelectrochemical activities, *Appl. Surf. Sci.*, **463**: 693-703(2019).
47. Q. Wang, P. Wang, P. Xu, Y. Li, J. Duan, G. Zhang, L. Hu, X. Wang and W. Zhang, Visible-light-driven photo-Fenton reactions using Zn1-1.5Fe S/g-C_3N_4 photocatalyst: Degradation kinetics and mechanisms analysis, *Appl. Catal. B Environ.*, **266**: 118653(2020).
48. A. Wang, H. Wang, H. Deng, S. Wang, W. Shi, Z. Yi, R. Qiu and K. Yan, Controllable synthesis of mesoporous manganese oxide microsphere efficient for photo-Fenton-like removal of fluoroquinolone antibiotics, *Appl. Catal. B Environ.*, **248**: 298-308(2019).
49. Z. Zhong, M. Li, J. Fu, Y. Wang, Y. Muhammad, S. Li, J. Wang, Z. Zhao and Z. Zhao, Construction of Cu-bridged Cu_2O/MIL(Fe/Cu) catalyst with enhanced interfacial contact for the synergistic photo-Fenton degradation of thiacloprid, *Chem. Eng. J.*, **395**: 125184(2020).